Joule

CellPress

Article

Uniform Permutation of Quasi-2D Perovskites by Vacuum Poling for Efficient, High-Fill-Factor Solar Cells

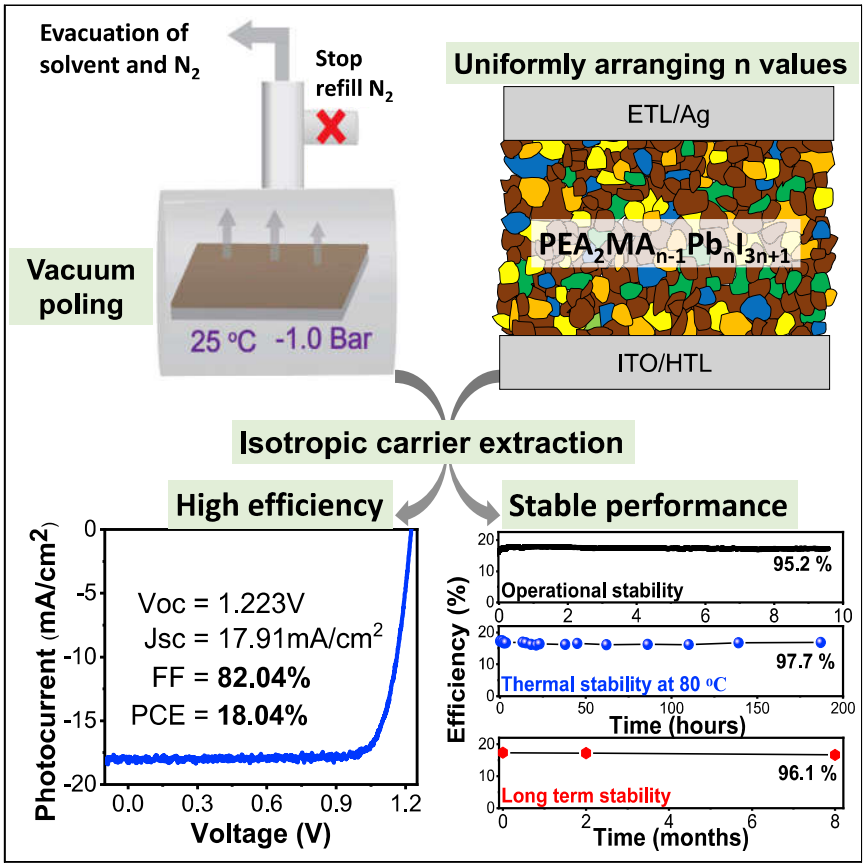

It is widely accepted that vertically aligning quasi-2D perovskites can improve power conversion efficiency due to directional charge transport from small to large-n-value nanoplates. Here, we report a different strategy of uniformly arranging different-n-value 2D nanoplates ($PEA_2MA_{n-1}Pb_nI_{3n+1}$) based on our vacuum poling method to enable superior isotropic carrier transport. Consequently, the high efficiency of 18.04% with open-circuit voltage of 1.223 V and champion fill-factor (FF) of 82.4% are demonstrated, presenting a new approach to develop advanced quasi-2D perovskite optoelectronic devices.

Jia Zhang, Jiajun Qin, Miaosheng Wang, ..., Haomiao Yu, Stefan Haacke, Bin Hu

bhu@utk.edu

HIGHLIGHTS

The uniform dispersion of different-n-value nanoplates is realized by vacuum poling

Tape-peeling-based optical studies confirm the uniform dispersion

Uniform dispersion enables highly efficient isotropic carrier collection

Uniform dispersion leads to high efficiency (18.04%) and champion FF (82.4%)

Zhang et al., Joule 3, 1–11
December 18, 2019
https://doi.org/10.1016/j.joule.2019.09.020

Please cite this article in press as: Zhang et al., Uniform Permutation of Quasi-2D Perovskites by Vacuum Poling for Efficient, High-Fill-Factor Solar Cells, Joule (2019), https://doi.org/10.1016/j.joule.2019.09.020

Joule

CellPress

Article

Uniform Permutation of Quasi-2D Perovskites by Vacuum Poling for Efficient, High-Fill-Factor Solar Cells

Jia Zhang,[1] Jiajun Qin,[2] Miaosheng Wang,[1] Yujie Bai,[2] Han Zou,[3] Jong Kahk Keum,[4] Runming Tao,[5] Hengxing Xu,[1] Haomiao Yu,[6] Stefan Haacke,[3] and Bin Hu[1,7,*]

SUMMARY

The vertically ordered (small-to-large n) quasi-2D perovskite films serve as common approaches to facilitate directional charge transfer. Here, we report a different strategy of uniformly arranging different-n-value nanoplates ($PEA_2MA_{n-1}Pb_nI_{3n+1}$) by introducing vacuum poling treatment to enforce nucleation during crystallization. This uniform distribution is verified by delicate mechanical tape-peeling method while monitoring optical absorption, photoluminescence (PL), and energy-dispersive X-ray spectroscopy (EDS). With uniform distribution, efficient carrier transfer within 10 ps is revealed by transient absorption. Moreover, record-high fill factor (FF) of 82.4% with power conversion efficiency (PCE) of 18.04% (Voc = 1.223 V, Jsc = 17.91 mA/cm^2) was demonstrated. Superior stability is achieved with retaining 96.1% of initial efficiency after 8-month storage and maintaining 97.7% at 80°C for over 180 h. This uniformly arranging different-n-value nanoplates offers a new material engineering strategy to enhance carrier transfer and extraction for developing high-efficiency and stable quasi-2D perovskite solar cells.

INTRODUCTION

Incorporation of long-chain organic ligands A′ has improved the optoelectronic performance[1–9] and stabilities[10–13] of perovskites by forming quasi-2D structures with the formula of $A'_2A_{n-1}M_nX_{3n+1}$, where n refers to the number of planes of the corner-sharing $[MX_6]^{4-}$ octahedral and A, M, and X refer to the monovalent cations, divalent metal cations, and halide anions, respectively. Remarkable tunability on optical properties via controlling morphological structures by selecting different functional A/A′ molecules has been shown to be a unique feature for quasi-2D perovskites.[3,4,10,14,15] However, with the incorporation of long-chain insulating organic ligands, carrier transport becomes a limiting factor in developing the optoelectronic properties. Vertically ordered small-n-value to large-n-value nanoplates between the bottom and top surfaces of the quasi-2D perovskite films are normally self-assembled based on unequal growth rates of different-n-value nanoplates, in which different amounts of organic ligands such as PEA^+ act as a barrier for mass transfer toward crystallization during thermal annealing.[1,2,16–18] Interestingly, such ordered-n-value dispersion in quasi-2D perovskite films provides an energy-cascade process to simultaneously transfer electrons and holes, consequently enhancing carrier transport.[1–4,8,19–21] These vertically ordered nanoplates of different n values have been shown to be the primary strategy to enhance photovoltaic[6,22] and light-emitting performance[1,2,20,21] in quasi-2D perovskite devices. In the present work, we demonstrate a uniform dispersion of different-n-value nanoplates as a new strategy

Context & Scale

2D nanoplates are normally vertically arranged from small to large n values in quasi-2D perovskite films, leading to ordered dispersion of different-n-value nanoplates to demonstrate efficient solar cells based on directional charge extraction. Here, we found a better choice that uniformly arranging different n-value nanoplates can be realized by using vacuum poling method to enable isotropic charge transfer from all small-n-value nanoplates directly to largest-n-value nanoplates. Essentially, this uniform dispersion is formed by mechanically enforcing nucleation during crystallization upon our vacuum poling method. Consequently, record-high fill factor (FF) of 82.4% with maximal power conversion efficiency of 18.04% (Voc = 1.223 V, Jsc = 17.91 mA/cm^2) is achieved with excellent stabilities. This work shows that uniformly arranging different-n-value nanoplates offers a new materials processing strategy for developing high-performance quasi-2D perovskite optoelectronic devices.

Please cite this article in press as: Zhang et al., Uniform Permutation of Quasi-2D Perovskites by Vacuum Poling for Efficient, High-Fill-Factor Solar Cells, Joule (2019), https://doi.org/10.1016/j.joule.2019.09.020

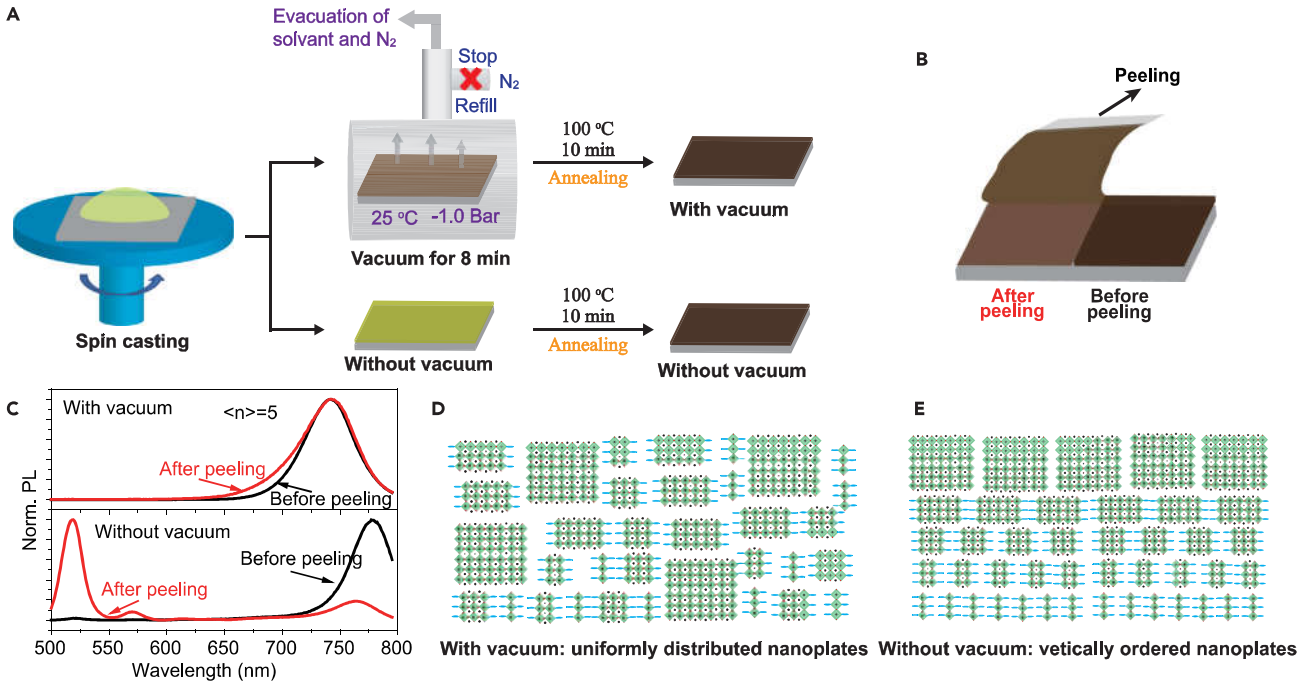

Figure 1. Schematic Diagram of Film Fabrication Procedure and Tape-Peeling-Based Photoluminescence Characterizations of Quasi-2D Perovskite Films Prepared with and without Vacuum Poling Treatment

(A) Schematic diagram to show processing methods with and without vacuum poling treatment to prepare quasi-2D perovskite films.

(B) Schematic drawing to illustrate our tape-peeling method, to mechanically detach monolayers from quasi-2D perovskite films, while subsequently measuring PL spectra, absorption, and EDS.

(C) PL spectra measured before and after peeling for <n> = 5 quasi-2D perovskite films prepared with and without vacuum poling treatment.

(D and E) Schematic diagrams to indicate uniform (D) and ordered (E) formation of different-n-value nanoplates in quasi-2D perovskite films prepared with and without vacuum poling treatment.

to enhance the optoelectronic properties of quasi-2D perovskites by using our vacuum poling treatment. Different from reported vacuum-assisted annealing method,[23,24] we developed our vacuum poling treatment to enforce nucleation during crystallization, leading to uniform dispersion of different-n-value nanoplates. With this new design, the charge transfer and carrier extraction are further improved toward developing high-performance quasi-2D perovskite solar cells.

RESULTS AND DISCUSSION

As schematically shown in Figure 1A, the precursor solutions with the stoichiometry designed to <n> = 5 are first spin-cast on preheated substrates to form a high density of nucleus. Then the films are immediately placed in a chamber for 8 min with the gage pressure quickly decreasing to −1.0 bar. Here, applying vacuum poling treatment can simultaneously increase the nucleation and limit the grain sizes by quickly removing residual solvent toward realizing uniform dispersion of different-n-value nanoplates. Afterward, thermal annealing is followed to further crystallize the 2D nanoplates at 100°C for 10 min in N_2 atmosphere. Consequently, high-quality quasi-2D perovskite films are formed with a uniform dispersion of different-n-value nanoplates. The competition between the crystallization and nucleation process during vacuum poling treatment is verified by absorption and photoluminescence (PL) results (Figure S1). In contrast, without vacuum poling treatment, the unaccelerated nucleation leads to the crystallization to form nanoplates with small n values on the bottom surface and large n values toward the top surface, creating vertically

[1]Department of Materials Science and Engineering, University of Tennessee, Knoxville, TN 37996, USA

[2]State Key Laboratory of Surface Physics, Key Laboratory of Micro and Nano Photonic Structures, Ministry of Education and Collaborative Innovation Center of Advanced Microstructures, Fudan University, Shanghai 200433, China

[3]University of Strasbourg – CNRS, UMR 7504, Institute de Physique et Chimie des Matériaux, 67034 Strasbourg, France

[4]Center for Nanophase Materials Science and Chemical and Engineering Materials Division, Oak Ridge National Laboratory, Oak Ridge, TN 37831, USA

[5]Department of Chemistry, Joint Institute for Advanced Materials, University of Tennessee, Knoxville, TN 37996, USA

[6]College of Science, Beijing Jiaotong University, Beijing 100044, China

[7]Lead Contact

*Correspondence: bhu@utk.edu

https://doi.org/10.1016/j.joule.2019.09.020

Please cite this article in press as: Zhang et al., Uniform Permutation of Quasi-2D Perovskites by Vacuum Poling for Efficient, High-Fill-Factor Solar Cells, Joule (2019), https://doi.org/10.1016/j.joule.2019.09.020

ordered (small-to-large n) dispersion of nanoplates in quasi-2D perovskite films under thermal annealing. Here, nuclear magnetic resonance (NMR) experiments[25] (Figures S2 and S3) show that vacuum poling treatment does not remove the ligands from the spin-cast film.

X-ray diffraction (XRD) patterns for quasi-2D perovskite films with uniform and ordered dispersions prepared with and without vacuum poling treatment are shown in Figure S4. With vacuum poling treatment, the XRD peaks around 14° and 28° are broader than that of the film without vacuum poling. Here, the lineshape broadening reflects the decreased grain sizes (evidenced by scanning electron microscopy [SEM] and atomic force microscopy [AFM] results in Figures S5 and S6) under uniform dispersion of different-n-value nanoplates. Especially, decreasing grain sizes can increase the probabilities to realize the uniform dispersion of different-n-value nanoplates.

To reveal the uniform dispersion of different-n-value nanoplates between bottom and top surfaces in quasi-2D perovskite films induced by vacuum poling treatment, we developed a delicate tape-peeling method (Figure 1B; the thicknesses for unpeeled and peeled films are ~300 and ~25 nm, respectively), to mechanically detach the multiple monolayers of nanoplates from top surface subsequently toward bottom surface while monitoring energy-dispersive X-ray spectroscopy (EDS), PL, and optical absorption, as shown in Figures S7, 1C, and S8.

Interestingly, the atomic ratio of Pb:C:I remains nearly the same after peeling off multiple monolayers for quasi-2D perovskite films prepared with vacuum poling treatment (Figure S7A). It indicates that the uniform dispersion of different-n-value nanoplates is realized between the bottom and top surfaces by using vacuum poling treatment. Moreover, with the mechanical tape-peeling method, very similar PL spectra with dominated peak at 740 nm (see upper figure of Figure 1C) and uniformly decreased absorption in the entire spectral range between 400 and 800 nm (Figures S8A and S8B) are observed after peeling off multiple monolayers of nanoplates from top surface toward bottom surface. These provide additional evidence of uniform distribution of nanoplates within quasi-2D perovskite films prepared with vacuum poling treatment.

In contrast, without vacuum poling treatment, EDS results in Figure S7B show that the ratio of C atoms increases after tape peeling, indicating more PEAI ligands (containing more C than MAI) on the bottom. Thus, the formation of an ordered distribution of nanoplates with small n value toward the bottom and large n value toward the top are suggested. Meanwhile, with mechanically tape-peeling method, very different PL spectra (see bottom figure of Figure 1C) are observed: the dominant PL peak locates at 778 nm related to large-n-value nanoplates before peeling and 519 nm related to small-n-value nanoplates after peeling, further proving the existence of ordered distribution of nanoplates. Moreover, after peeling off the multiple monolayers of film prepared without vacuum poling treatment, the absorption spectrum shows two dominant peaks at around 516 nm and 566 nm related to n = 1 and n = 2 nanoplates (Figure S8B), providing further evidence of the vertically ordered distribution of nanoplates. In addition, it should be noted that the coexistence of multiple PL peaks indicates that the charge transfer is not efficient between nanoplates with ordered-n-value dispersion. The spatial distribution of different-n-value nanoplates are illustrated in Figures 1D and 1E.

To discuss the dynamics of charge transfer in quasi-2D perovskite films, transient absorption (TA) measurements were carried out. With the vacuum poling treatment,

Please cite this article in press as: Zhang et al., Uniform Permutation of Quasi-2D Perovskites by Vacuum Poling for Efficient, High-Fill-Factor Solar Cells, Joule (2019), https://doi.org/10.1016/j.joule.2019.09.020

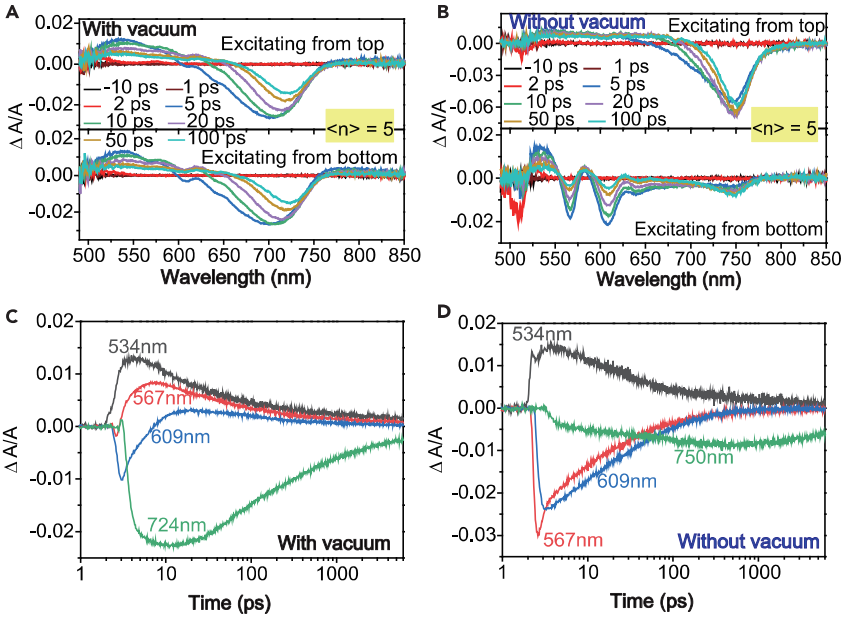

Figure 2. Characteraction of Carrier Transfer Dynamics of Quasi-2D Perovskites Prepared with and without Vacuum Poling Treatment

Transient absorption (TA) spectra at different delay times (−10, 1, 2, 5, 10, 20, 50, and 100 ps) and dynamics of quasi-2D perovskite (<n> = 5) films when exciting through the top (upper figures of A and B) and bottom (down figures of A and B). The wavelengths at 534, 567, 609, and 724 nm (750 nm) correspond to signals from small-n-value to largest-n-value nanoplates.

(A) With vacuum poling treatment. TA spectra are similar when exciting through the top (upper figure) and bottom (lower figure), indicating the uniform distribution of nanoplates.

(B) Without vacuum poling treatment. TA spectra are quite different when exciting through the top (upper figure) and bottom (lower figure), indicating order dispersion of nanoplates.

(C) <n> = 5 film with vacuum poling treatment shows positive transient absorption signals at small-n-value nanoplates and fast (within 10 ps) increased negative signal at 724 nm (corresponding to largest-n-value nanoplates).

(D) <n> = 5 film without vacuum poling treatment shows both positive (at 534 nm) and negative (at 567 and 609 nm) transient absorption signals at small-n-value nanoplates and slow (~600 ps) increased negative signal at 750 nm (corresponding to largest-n-value nanoplates).

the TA measured through top and bottom shows similar characteristics, as shown in Figure 2A, further verifying the uniform dispersion of different-n-value nanoplates. Without vacuum poling treatment, the TA measured through top and bottom show very different characteristics (Figure 2B), verifying that smaller-n-value and larger-n-value nanoplates are distributed toward bottom and top, respectively. This is consistent with the publication of other ordered quasi-2D perovskite films.[7] Moreover, TA dynamics at wavelengths at 534, 567, 609, and 724 nm (or 750 nm) corresponding to signals from small-n-value to largest-n-value nanoplates are plotted in Figures 2C and 2D. It is shown that vacuum poling treatment leads to a fast increment within 10 ps on the negative ΔA/A signal at 724 nm in Figure 2C (corresponding to largest-n-value nanoplates). In the meantime, positive ΔA/A signals at other wavelengths are observed, indicating that the charge transfer from small-n-value nanoplates to largest-n-value nanoplates is very efficient without much accumulations between nanoplates. In contrast, without vacuum poling treatment, the negative ΔA/A signal (750 nm in Figure 2D, corresponding to largest-n-value nanoplates) shows a much slower increment within 600 ps (Figure 2D), while negative ΔA/A signals also appear at 567 and 609 nm. It implies that accumulations of charge carriers occur at corresponding small-n-value nanoplates (567 and

Please cite this article in press as: Zhang et al., Uniform Permutation of Quasi-2D Perovskites by Vacuum Poling for Efficient, High-Fill-Factor Solar Cells, Joule (2019), https://doi.org/10.1016/j.joule.2019.09.020

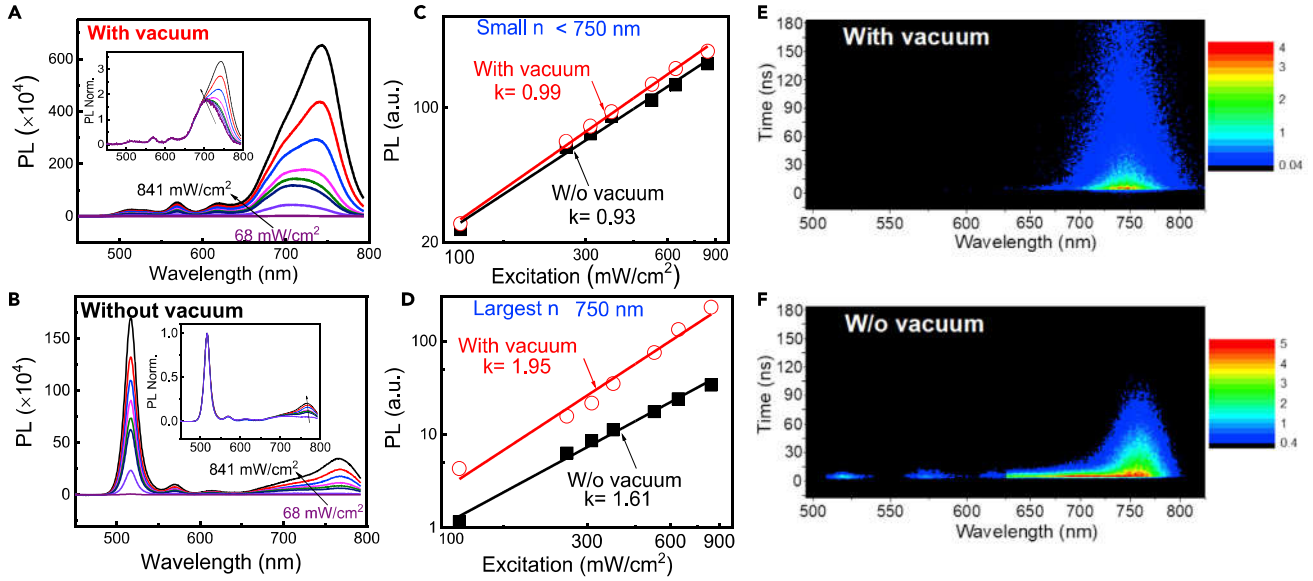

Figure 3. PL Characterizations and Dynamics for Quasi-2D Perovskite=5) Films Prepared with and without Vacuum Poling Treatment

(A and B) PL spectra for quasi-2D perovskite films prepared with (A) and without vacuum (B) poling treatment.

(C) PL-excitation intensity dependences for emission peaks ≤710 nm related to small n-value nanoplates prepared with and without vacuum poling treatment.

(D) PL-excitation intensity dependences (at 750 nm) for the largest n-value nanoplates prepared with and without vacuum poling treatment.

(E and F) PL dynamics for quasi-2D perovskite films prepared with and without vacuum poling treatment. Sample structure: ITO/PEDOT:PSS/Perovskites. Excitation: 346 nm pulsed laser (pulse width of 290 fs) with an intensity of 5 μW.

609 nm), leading to less efficient charge transfer in the ordered dispersion of different-n-value nanoplates prepared without vacuum poling treatment. It should be noted that vacuum poling method can also be applied to other quasi-2D perovskite films prepared with average n values such as <n> = 4 and 3 for obtaining uniform distribution of nanoplates, as evidenced by TA spectra (Figure S9) exciting through different sides and tape-peeling based PL results (Figure S10).

To further understand the dynamics of photoexcited states under uniform and ordered dispersions of different-n-value nanoplates, PL characteristics were analyzed for quasi-2D perovskite films prepared with and without vacuum poling treatment. Under both conditions, the PL spectra consist of various peaks originating from different n-value nanoplates (n = 1, 2, 3, 4, n > 4) peaked at around 518, 570, 612, 710, and 750 nm, as shown in Figures 3A and 3B. However, with vacuum poling, increasing the photoexcitation intensity at 405 nm significantly increases the light emission from the largest-n-value nanoplates (n > 4), while the light emission from small n values (n ≤ 4) are slightly increased (see the inset of Figure 3A). This intensity-dependent PL[20,21] indicates that the uniform dispersion of different-n-value nanoplates generates efficient transport of photogenerated carriers (can also be evidenced by power-dependent PL and EL; Figure S11) from small to large n-value nanoplates in quasi-2D perovskite films prepared with vacuum poling treatment. Contrarily, without vacuum poling, increasing excitation intensity mainly increases the light emission from small-n-value nanoplates dominated by n = 1 (Figure 3B). This implies that the transport of photogenerated carriers is less efficient in the ordered dispersion of different-n-value nanoplates.

Moreover, we notice that the vacuum poling treatment increases the slope of PL-excitation intensity dependence from 1.61 to 1.95 toward ideal bimolecular recombination in the large-n-value nanoplates with emission at 750 nm, but the slope

Please cite this article in press as: Zhang et al., Uniform Permutation of Quasi-2D Perovskites by Vacuum Poling for Efficient, High-Fill-Factor Solar Cells, Joule (2019), https://doi.org/10.1016/j.joule.2019.09.020

almost keeps unchanged in small-n-value nanoplates, with emission peaking at around 518, 570, 612, and 710 nm (shown in Figures 3C and 3D). This phenomenon may imply that small-n-value nanoplates can function as passivation agents and largest-n-value nanoplates as the emitting centers, which is similar to our recent observation that small grains can passivate the defects on the surfaces of large grains in hybrid perovskites.[26,27] In quasi-2D perovskite films with uniform distribution of nanoplates, large-n-value nanoplates are surrounded by small-n-value nanoplates, which enables more contacts for passivation than ordered dispersion of nanoplates (the films without vacuum poling treatment). As a consequence, the quasi-2D perovskite films with uniform dispersion of different-n-value nanoplates demonstrate longer PL lifetime, as compared to the ordered dispersion (Figure S12). TRPL data detected with the Streak camera in Figures 3E and 3F further indicate the prolonged PL lifetime under vacuum poling treatment. Clearly, the uniform dispersion of nanoplates shows one major emission peak at 750 nm with a longer lifetime, while the ordered nanoplates show multiple emission peaks with shorter PL lifetimes.

To understand the carrier extraction mechanism under uniform dispersion of different-n-value nanoplates based on vacuum poling treatment, the photovoltaic performance was characterized based on the device architecture of ITO/PTAA/$PEA_2MA_{n-1}Pb_nI_{3n+1}$/$PC_{61}BM$/PEI/Ag. As shown in Figure 4A, the vacuum poling treatment leads to the record-high FF of 82.4% with the PCE reaching 18.04% (Voc = 1.223 V, Jsc = 17.91 mA/cm^2), indicating extremely efficient carrier extraction under the uniform dispersion of different-n-value nanoplates. For comparison, we also fabricated devices without vacuum poling treatment using PEDOT: PSS as hole transport layer (HTL) (short circuit occurs in without-vacuum-treated devices due to pinholes when using PTAA as HTL). The I-V curves of best-performing devices with and without vacuum treatment (PEDOT: PSS as HTL) are compared in Figure S13. When replacing PEDOT: PPS with PTAA in vacuum-treated devices, the decreased dark current and increased PL lifetime (Figure S14; Table S1) account for the better photovoltaic performance of PTAA-based devices.

External quantum efficiency (EQE) results are shown in Figure S15, and the corresponding integrated Jsc of devices with and without vacuum poling treatment is 18.09 and 17.79 mA/cm^2, respectively. It is noted that the quasi-2D perovskite films prepared with vacuum poling treatment shows the bandgap of 1.60 eV, slightly wider than the band gap of 1.57 eV prepared without vacuum poling treatment (Figure S8C). Clearly, the photovoltaic enhancement enabled by vacuum poling method does not result from absorption, which further verifies more efficient transport of photogenerated carriers responsible for the record-high fill factor (FF) and efficiency.

It is well known that using different organic ligands and transport-layer engineering can improve the FF of quasi-2D perovskite solar cells.[11,13,28–34] Here, we compare the solar cells prepared by our vacuum poling treatment with the devices prepared using published conventional non-vacuum method. Clearly, the FF of our champion devices is the highest among published quasi-2D perovskite solar cells (Figure 4B). For quasi-2D perovskites of <n> = 3 and 4, vacuum poling treatment also leads to high photovoltaic efficiency with high FF and open-circuit voltage (Figure S16; Table S2). It further verifies that the uniform dispersion of nanoplates is responsible for highly efficient carrier extraction. Moreover, the upper curve of Figure 4C shows the output efficiency at maximum power point (MPP) monitored continuously without device encapsulation. The PCE remains as high as 95.2% of the maximum

Please cite this article in press as: Zhang et al., Uniform Permutation of Quasi-2D Perovskites by Vacuum Poling for Efficient, High-Fill-Factor Solar Cells, Joule (2019), https://doi.org/10.1016/j.joule.2019.09.020

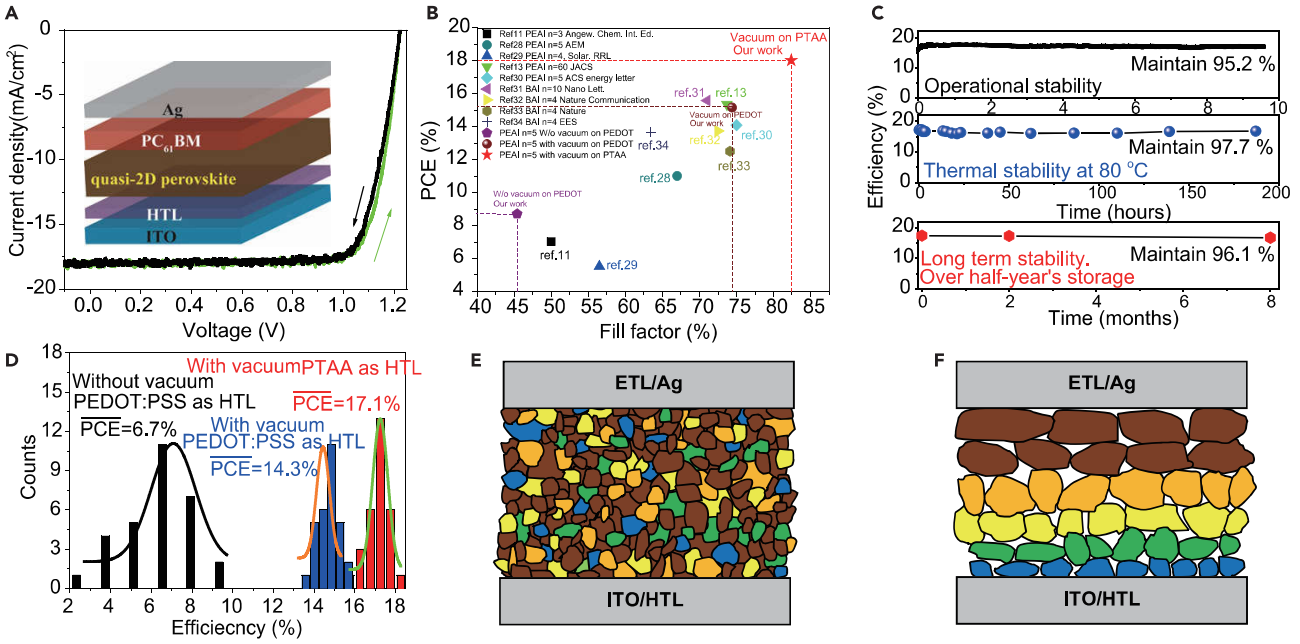

Figure 4. Characterizations and Schematic Diagram of Quasi-2D Perovskite=5) Solar Cells Prepared with/without Vacuum Poling Treatment

Different-n-value nanoplates are schematically shown with different colors: blue and green areas corresponding to small-n-value nanoplates, yellow and orange areas representing medium-n-value nanoplates, and brown areas indicating largest-n-value nanoplates.

(A) I-V characteristics measured under 1 Sun illumination in quasi-2D perovskite solar cells prepared with vacuum poling treatment (PTAA used as HTL).

(B) Photovoltaic performance (FF and PCE) of our device as compared with published PEA^+ and BA^+ based quasi-2D perovskite solar cells. Our vacuum poling treatment leads to extremely high FF and PCE.

(C) Device stability tests of quasi-2D perovskite device prepared with vacuum poling treatment (HTL: PTAA) under various conditions. Upper figure, operational stability under continuous 1-sun illumination; middle figure, thermal stability at 80°C; bottom figure, over half-year long-term stability stored in the glovebox.

(D) Statistics data of the photovoltaic performance of quasi-2D perovskite solar cells with three different designs: without vacuum poling on PEDOT: PSS, with vacuum poling on PEDOT: PSS and with vacuum poling on PTAA.

(E) Schematic diagram to show isotropic carrier extraction from all small-n-value nanoplates directly to largest-n-value nanoplates functioning as transport highway (shown in brown color) under uniform dispersion of different-n-value nanoplates in our quasi-2D perovskite solar cells prepared with vacuum poling treatment.

(F) Schematic diagram to show less efficient and prolonged carrier extraction time from n = 1 to n = 2, n = 3, n = 4, and n = 5 nanoplates through cascade process under ordered dispersion of different-n-value nanoplates in our quasi-2D perovskite solar cells prepared without vacuum poling treatment.

point after more than 9.5 h, indicating considerably improved operational stability at continuous working conditions, as compared with 3D-only and without-vacuum-poling-treated control devices (Figures S17 and S18). More surprisingly, after heating the device at 80°C for over 180 h, the PCE maintains 97.7% (see the middle curve of Figure 4C) of its original value for quasi-2D perovskite devices prepared with vacuum poling treatment, which indicates extremely good thermal stability. For comparison, the 3D-only devices and quasi-2D devices without vacuum poling treatment drastically drop their PCE within 1 h at 80°C (Figure S19). In addition, the device efficiency retains 96.1% of original value after storing in glove box for 8 months without encapsulation (see down curve of Figure 4C). The statistics data in Figures 4D, S20, and S21 show that vacuum poling treatment significantly improves the reproducibility of device performance. In contrast, devices fabricated without vacuum poling treatment suffer from poorer performance and lower reproducibility (Figure S22).

As schematically shown in Figure 4E, the uniform dispersion increases the contact probabilities between different-n-value nanoplates to generate isotropic transport from all small-n-value nanoplates directly to largest-n-value nanoplates.

Please cite this article in press as: Zhang et al., Uniform Permutation of Quasi-2D Perovskites by Vacuum Poling for Efficient, High-Fill-Factor Solar Cells, Joule (2019), https://doi.org/10.1016/j.joule.2019.09.020

Consequently, photogenerated carriers are isotropically transported from small-n-value nanoplates to largest-n-value nanoplates in all directions in quasi-2D perovskite films prepared with uniform dispersion of nanoplates. It should be emphasized that the uniform dispersion can decrease the transport time to collect photogenerated carriers because all photogenerated carriers in small-n-value nanoplates have an opportunity to directly transport to largest-n-value nanoplates (functioning as a transport-highway network) due to the increased contact probabilities between different-n-value nanoplates. Therefore, a record-high FF (82.4%) is demonstrated in our work. In contrast, in ordered dispersion, the photogenerated carriers are cascaded from n = 1 to n = 2, n = 3, n = 4, n = 5 nanoplates, leading to a prolonged time to collect photogenerated carriers through such cascade process. In ordered dispersion (Figure 4F), large-n-value nanoplates do not form a continuous network vertically, consequently lacking the transport highway to more effectively collect photogenerated carriers.

Conclusions

In summary, we explored the uniform dispersion of different-n-value nanoplates homogenously located between bottom and top surfaces in quasi-2D perovskite films [$(PEA)_2(MA)_{n-1}Pb_nI_{3n+1}$] by introducing vacuum poling treatment. In contrast, without vacuum poling treatment, the different-n-value nanoplates are formed with vertically ordered dispersion from small to large n values between the bottom and top surfaces in quasi-2D perovskite films. The uniform and ordered dispersions of different-n-value nanoplates between the bottom and top surfaces were verified by our tape-peeling method to mechanically detach monolayers of nanoplates from top surface subsequently toward the bottom surface while monitoring the EDS, PL spectra, and optical absorption. The TA results showed that the uniform dispersion of different-n-value nanoplates leads to a fast charge transfer toward the largest-n-value nanoplates within 10 ps. The PL dynamics studies implied that with vacuum poling-enabled uniform dispersion, small-n-value and large-n-value nanoplates may function as passivation agents and light-emitting centers, respectively, in quasi-2D perovskite films with enhanced PL intensity and lifetime. Furthermore, with uniform dispersion of different-n-value nanoplates, the quasi-2D perovskite solar cells demonstrate a record-high FF (82.4%) with maximum PCE of 18.04% (Jsc = 17.91 mA/cm^2 and Voc = 1.223 V) based on the device structure of ITO/PTAA/$PEA_2MA_{n-1}Pb_nI_{3n+1}$/$PC_{61}BM$/PEI/Ag. Surprisingly, superior stabilities are achieved with retaining over 96% of their initial efficiency after storing for 8 months and 97.7% of the original value at 80°C for over 180 h. Therefore, uniformly arranging different-n-value nanoplates through vacuum poling treatment provides a new strategy to enhance carrier extraction toward developing high-performance quasi-2D perovskite optoelectronics.

EXPERIMENTAL PROCEDURES

Materials Processing and Device Fabrication

The ITO substrates were cleaned by ultrasonic treatment with detergent, deionized water, acetone, and isopropanol, subsequently, for 20 min in each cycle. After cleaning, the ITO substrates were exposed to UV ozone for 30 min and followed by spin-coating PEDOT: PSS with a thickness of 40 nm or PTAA with a thickness of 10 nm. The PEDOT: PSS (Clevious PVP AI 4083) films coated at the rate of 4,000 rpm for 1 min were thermally annealed at 150°C for 0.5 h; the PTAA (1.5 mg/mL in toluene) was spin-cast at the rate of 2,000 rpm for 1 min followed by thermal annealing at 110°C for 10 min.

The precursor solution with the target of <n> = 5 quasi-2D perovskites was prepared by the mixture of PEAI:MAI:PbI_2:$PbCl_2$ with a molar ratio of 0.4:0.9:0.95:0.05 in the

mixed solvent of DMF:DMSO (9:1 vol). The stoichiometric ratios to prepare <n> = 4 and <n> = 3 perovskites are 0.5 M (PEAI): 0.85 M (MAI): 0.95 M (PbI_2): 0.05 M ($PbCl_2$) and 0.67 M (PEAI): 0.77 M (MAI): 0.95 M (PbI_2): 0.05 M ($PbCl_2$), respectively. It should be noted that *in situ* MACl additives were introduced through the reaction of $0.05PbCl_2 + 0.1MAI = 0.05PbI_2 + 0.1MACl$ for better crystallization and improved film quality.[35,36] During the crystallization, different n-value nanoplates are co-grown to form quasi-2D perovskite films during spin-coating. The concentrations for perovskite precursor solutions used for the PEDOT: PSS and PTAA-based devices were 1 and 0.7 M of Pb^{2+}, respectively. All precursor solutions (200 μL) were spin-cast on the preheated substrates (100°C for over 20 min) at the rate of 5,000 rpm for 20 s, followed by vacuum poling of 8 min in a vacuum chamber where the gage pressure is quickly reduced to −1 bar within 14 s to initiate vacuum poling effects. It should be noted that to delay the crystallization during the spin-coating process, *in situ* MACl and additional DMSO were intentionally introduced in the precursor solution. Moreover, before starting spin-coating, we dropped a large amount of cold precursor solution (200 μL) onto the preheated substrate (1.5 × 1.5 cm) to further delay crystallization during the spin-coating. After thermal annealing, all samples including quasi-2D perovskites prepared with and without vacuum poling were thermally annealed at 100°C for 10 min. The electron transport layer phenyl-C_{61}-butyric acid methyl ester ($PC_{61}BM$, 20 mg/mL in chlorobenzene) was spin-cast on top of perovskite films at 2,000 rpm for 50 s and kept in dark for at least 60 min before the coating of an interface-modifying layer PEI (0.5 mg/mL, in anhydride 2-propanol) at 5,000 rpm for 60 s. Finally, these films were transferred into a thermal evaporator for the deposition of 90-nm-thick silver electrodes under a vacuum of 2×10^{-4} Pa. The 3D-only perovskite control devices are fabricated with the same device architecture following our previous procedure.[37]

Characterizations and Measurements

For the tape-peeling method, the thicknesses for unpeeled and peeled films are ~300 and ~25 nm, respectively, for quasi-2D perovskite film, confirmed by atomic force microscopy (AFM). For NMR measurement, solvent dimethyl sulfoxide-d6 (DMSO-D6) was purchased from commercial vendors and used without further purification. ^1H spectra were recorded at ambient temperature on a JEOL 400YH spectrometer, and ^1H NMR chemical shifts were referenced to the residual solvent. For SEM-EDS mapping, scanning electron microscope (SEM) energy-dispersive X-ray spectroscopies (EDS) mapping[38] was conducted on a Hitachi High-Technologies TM3030Plus SEM microscope at 15 kV.

Transient absorption spectra were collected by using a Helios fire spectrometer (Ultrafast Systems LLC). The pump pulses (346 nm, 5 μW) were generated through a harmonic generator (Ultrafast Systems LLC, third harmonic) pumped by a Pharos laser (Light Conversion, 1 kHz, 1,030 nm, 290 fs). The 346 nm pump beam was focused into point on the samples with the diameter of ~100 μm.

The device active area is 0.06 cm^2, which is realized by a shadow mask. The current-voltage (I-V) characteristics of the solar cells were measured by scanning the voltage from −0.1 to 1.25 V (forward scan) and then from 1.25 to −0.1 V (reverse scan) with 0.68 mV step and NPLC = 0.001. The I-V characteristics were recorded by using Keithley 2400 source meter under the illumination of AM 1.5G 100 mW/cm^2 from Newport solar simulator calibrated by a silicon reference cell. Operational stability tests were operated under constant bias at maximum power point in nitrogen glove box. Thermal stability tests were operated by placing the device on the hotplate with temperature at 80°C.

The absorption spectrum is measured with an integrating sphere system (R7, ideaoptics, China) equipped with spectrometers (PG2,000-Pro, NIR1,700, ideaoptics, China). The external quantum efficiency (EQE) spectra were measured by subjecting the cells to a monochromatic illumination (300 W Xe lamp passing through a monochromator and appropriate filters). The light intensity was calibrated by a standard Si-based photodetector (DET100A, 350–1,100 nm, Thor Labs). The light beam was chopped at 230 Hz, and the response of the cell was acquired by a Stanford Research SR830 lock-in amplifier. The PL lifetimes were measured by Streak camera (HAMAMATSU C10627) by exciting the samples with a 346 nm pulse laser (300 fs per pulse) generated by noncollinear optical parametric amplifier (NOPA) seeded by the second harmonic of a Yb-doped fiber laser (TANGERINE, Amplitude System) with 50 kHz repetition rate and the average power of 10 μW.

SUPPLEMENTAL INFORMATION

Supplemental Information can be found online at https://doi.org/10.1016/j.joule.2019.09.020.

ACKNOWLEDGMENTS

The authors at the University of Tennessee acknowledge funding support from the Air Force Office of Scientific Research (AFOSR) under the grant number FA 9550-15-1-0064, AOARD (FA2386-15-1-4104), and National Science Foundation (NSF-1911659). This research was partially performed at the Center for Nanophase Materials Sciences based on user projects (CNMS2017-102), which is sponsored by Oak Ridge National Laboratory by the Division of Scientific User Facilities, U.S. Department of Energy.

AUTHOR CONTRIBUTIONS

Conceptualization and Methodology, J.Z.; Validation, B.H. and J.Z.; Investigation, J.Z., J.Q., M.W., Y.B., H.Z., J.K.K., R.T., H.X., and H.Y.; Writing – Original Draft, J.Z.; Writing – Review & Editing, B.H. and J.Q.; Supervision, B.H.

DECLARATION OF INTERESTS

The authors declare no competing interests.

Received: July 10, 2019
Revised: August 27, 2019
Accepted: September 26, 2019
Published: October 22, 2019

REFERENCES

1. Yuan, M., Quan, L.N., Comin, R., Walters, G., Sabatini, R., Voznyy, O., Hoogland, S., Zhao, Y., Beauregard, E.M., Kanjanaboos, P., et al. (2016). Perovskite energy funnels for efficient light-emitting diodes. Nat. Nanotechnol. *11*, 872–877.

2. Wang, N., Cheng, L., Ge, R., Zhang, S., Miao, Y., Zou, W., Yi, C., Sun, Y., Cao, Y., Yang, R., et al. (2016). Perovskite light-emitting diodes based on solution-processed self-organized multiple quantum wells. Nat. Photonics *10*, 699–704.

3. Chen, Z., Guo, Y., Wertz, E., and Shi, J. (2019). Merits and challenges of Ruddlesden-Popper soft halide perovskites in electro-optics and optoelectronics. Adv. Mater. *31*, 1803514–1803532.

4. Hu, J., Yan, L., and You, W. (2018). Two-dimensional organic-inorganic hybrid perovskites: a new platform for optoelectronic applications. Adv. Mater. *30*, 1802041–1802051.

5. Quintero-Bermudez, R., Gold-Parker, A., Proppe, A.H., Munir, R., Yang, Z., Kelley, S.O., Amassian, A., Toney, M.F., and Sargent, E.H. (2018). Compositional and orientational control in metal halide perovskites of reduced dimensionality. Nat. Mater. *17*, 900–907.

6. Proppe, A.H., Quintero-Bermudez, R., Tan, H., Voznyy, O., Kelley, S.O., and Sargent, E.H. (2018). Synthetic control over quantum well width distribution and carrier migration in low-dimensional perovskite photovoltaics. J. Am. Chem. Soc. *140*, 2890–2896.

7. Liu, J., Leng, J., Wu, K., Zhang, J., and Jin, S. (2017). Observation of internal photoinduced electron and hole separation in hybrid two-dimentional perovskite films. J. Am. Chem. Soc. *139*, 1432–1435.

8. Shang, Q., Wang, Y., Zhong, Y., Mi, Y., Qin, L., Zhao, Y., Qiu, X., Liu, X., and Zhang, Q. (2017). Unveiling structurally engineered carrier dynamics in hybrid quasi-two-dimensional

perovskite thin films toward controllable emission. J. Phys. Chem. Lett. *8*, 4431–4438.

9. Kagan, C.R., Mitzi, D.B., and Dimitrakopoulos, C.D. (1999). Organic-inorganic hybrid materials as semiconducting channels in thin-film field-effect transistors. Science *286*, 945–947.

10. Chen, Y., Sun, Y., Peng, J., Tang, J., Zheng, K., and Liang, Z. (2018). 2D Ruddlesden-Popper perovskites for optoelectronics. Adv. Mater. *30*, 1703847–1703862.

11. Smith, I.C., Hoke, E.T., Solis-Ibarra, D., McGehee, M.D., and Karunadasa, H.I. (2014). A layered hybrid perovskite solar-cell absorber with enhanced moisture stability. Angew. Chem. *126*, 11414–11417.

12. Grancini, G., Roldán-Carmona, C., Zimmermann, I., Mosconi, E., Lee, X., Martineau, D., Narbey, S., Oswald, F., De Angelis, F., Graetzel, M., et al. (2017). One-year stable perovskite solar cells by 2D/3D interface engineering. Nat. Commun. *8*, 15684.

13. Quan, L.N., Yuan, M., Comin, R., Voznyy, O., Beauregard, E.M., Hoogland, S., Buin, A., Kirmani, A.R., Zhao, K., Amassian, A., et al. (2016). Ligand-stabilized reduced-dimensionality perovskites. J. Am. Chem. Soc. *138*, 2649–2655.

14. Xiao, Z., Zhao, L., Tran, N.L., Lin, Y.L., Silver, S.H., Kerner, R.A., Yao, N., Kahn, A., Scholes, G.D., and Rand, B.P. (2017). Mixed-halide perovskites with stabilized bandgaps. Nano Lett. *17*, 6863–6869.

15. Peng, W., Yin, J., Ho, K.T., Ouellette, O., De Bastiani, M., Murali, B., El Tall, O., Shen, C., Miao, X., Pan, J., et al. (2017). Ultralow self-doping in two-dimensional hybrid perovskite single crystals. Nano Lett. *17*, 4759–4767.

16. Qin, J., Zheng, Y., Xia, Y., Chao, L., Chen, Y., and Huang, W. (2018). Rapid crystallization for efficient 2D Ruddlesden–Popper (2DRP) perovskite solar cells. Adv. Funct. Mater. Published online December 13, 2018. https://doi.org/10.1002/adfm.201806831.

17. Xue, C., Shi, Y., Zhang, C., Lv, Y., Feng, Y., Tian, W., Jin, S., and Ma, T. (2019). Favorable growth of well-crystallized layered hybrid perovskite by combination of thermal and solvent assistance. J. Power Sources *422*, 156–162.

18. Soe, C.M.M., Nie, W., Stoumpos, C.C., Tsai, H., Blancon, J.-C., Liu, F., Even, J., Marks, T.J., Mohite, A.D., and Kanatzidis, M.G. (2018). Understanding film formation morphology and orientation in high member 2D Ruddlesden-Popper perovskites for high-efficiency solar cells. Adv. Energy Mater. *8*, 1700979.

19. Wang, J., Leng, J., Liu, J., He, S., Wang, Y., Wu, K., and Jin, S. (2017). Engineered directional charge flow in mixed two-dimensional perovskites enabled by facile cation-exchange. J. Phys. Chem. C *121*, 21281–21289.

20. Chen, P., Meng, Y., Ahmadi, M., Peng, Q., Gao, C., Xu, L., Shao, M., Xiong, Z., and Hu, B. (2018). Charge-transfer versus energy-transfer in quasi-2D perovskite light-emitting diodes. Nano Energy *50*, 615–622.

21. Quan, L.N., Zhao, Y., Garcia de Arquer, F.P., Sabatini, R., Walters, G., Voznyy, O., Comin, R., Li, Y., Fan, J.Z., Tan, H., et al. (2017). Tailoring the energy landscape in quasi-2D halide perovskites enables efficient green-light emission. Nano Lett. *17*, 3701–3709.

22. Yang, R., Li, R., Cao, Y., Wei, Y., Miao, Y., Tan, W.L., Jiao, X., Chen, H., Zhang, L., Chen, Q., et al. (2018). Oriented quasi-2D perovskites for high performance optoelectronic devices. Adv. Mater. *30*, 1804771–1804779.

23. Xie, F.X., Zhang, D., Su, H., Ren, X., Wong, K.S., Grätzel, M., and Choy, W.C.H. (2015). Vacuum-assisted thermal annealing of $CH_3NH_3PbI_3$ for highly stable and efficient perovskite solar cells. ACS Nano *9*, 639–646.

24. Li, X., Bi, D., Yi, C., Décoppet, J.D., Luo, J., Zakeeruddin, S.M., Hagfeldt, A., and Grätzel, M. (2016). A vacuum flash–assisted solution process for high-efficiency large-area perovskite solar cells. Science *353*, 58–62.

25. Yan, L., Hu, J., Guo, Z., Chen, H., Toney, M.F., Moran, A.M., and You, W. (2018). General post-annealing method enables high-efficiency two-dimensional perovskite solar cells. ACS Appl. Mater. Interfaces *10*, 33187–33197.

26. Qin, J., Zhang, J., Bai, Y., Ma, S., Wang, M., Xu, H., et al. (2019). Enabling self-passivation by attaching small grains on surfaces of large grains toward high-performance perovskite LEDs. iScience *19*, 378–387.

27. Bai, Y., Qin, J., Shi, L., Zhang, J., Wang, M., Zhan, Y., Zou, H., Haacke, S., Hou, X., Zi, J., et al. (2019). Amplified spontaneous emission realized by cogrowing large/small grains with self-passivating defects and aligning transition dipoles. Adv. Opt. Mater. *7*, 1900345.

28. Zhang, X., Wu, G., Fu, W., Qin, M., Yang, W., Yan, J., Zhang, Z., Lu, X., and Chen, H. (2018). Orientation regulation of phenylethylammonium cation based 2D perovskite solar cell with efficiency higher than 11%. Adv. Energy Mater. *8*, 1702498–1702507.

29. Thrithamarassery Gangadharan, D., Han, Y., Dubey, A., Gao, X., Sun, B., Qiao, Q., Izquierdo, R., and Ma, D. (2018). Aromatic alkylammonium spacer cations for efficient two-dimensional perovskite solar cells with enhanced moisture and thermal stability. Sol. RRL *2*, 1700215–1700225.

30. Fu, W., Wang, J., Zuo, L., Gao, K., Liu, F., Ginger, D.S., and Jen, A.K.-Y. (2018). Two-dimensional perovskite solar cells with 14.1% power conversion efficiency and 0.68% external radiative efficiency. ACS Energy Lett. *3*, 2086–2093.

31. Cohen, B.E., Li, Y., Meng, Q., and Etgar, L. (2019). Dion-Jacobson two-dimensional perovskite solar cells based on benzene dimethanammonium cation. Nano Lett. *19*, 2588–2597.

32. Liu, T., Jiang, Y., Qin, M., Liu, J., Sun, L., Qin, F., Hu, L., Xiong, S., Jiang, X., Jiang, F., et al. (2019). Tailoring vertical phase distribution of quasi-two-dimensional perovskite films via surface modification of hole-transporting layer. Nat. Commun. *10*, 878.

33. Tsai, H., Nie, W., Blancon, J.C., Stoumpos, C.C., Asadpour, R., Harutyunyan, B., Neukirch, A.J., Verduzco, R., Crochet, J.J., Tretiak, S., et al. (2016). High-efficiency two-dimensional Ruddlesden-Popper perovskite solar cells. Nature *536*, 312–316.

34. Zhang, X., Ren, X., Liu, B., Munir, R., Zhu, X., Yang, D., et al. (2017). Stable high efficiency two-dimensional perovskite solar cells via cesium doping. Energy Environ. Sci. *10*, 2095–2102.

35. Qing, J., Liu, X.-K., Li, M., Liu, F., Yuan, Z., Tiukalova, E., Yan, Z., Duchamp, M., Chen, S., Wang, Y., et al. (2018). Aligned and graded type-II Ruddlesden-Popper perovskite films for efficient solar cells. Adv. Energy Mater. *8*, 1800185.

36. Lai, H., Kan, B., Liu, T., Zheng, N., Xie, Z., Zhou, T., Wan, X., Zhang, X., Liu, Y., and Chen, Y. (2018). Two-dimensional Ruddlesden-Popper perovskite with nanorod-like morphology for solar cells with efficiency exceeding 15. J. Am. Chem. Soc. *140*, 11639–11646.

37. Zhang, J., Wu, T., Duan, J., Ahmadi, M., Jiang, F., Zhou, Y., and Hu, B. (2017). Exploring spin-orbital coupling effects on photovoltaic actions in Sn and Pb based perovskite solar cells. Nano Energy *38*, 297–303.

38. Cao, D.H., Stoumpos, C.C., Farha, O.K., Hupp, J.T., and Kanatzidis, M.G. (2015). 2D Homologous perovskites as light-absorbing materials for solar cell applications. J. Am. Chem. Soc. *137*, 7843–7850.